scientific reports

Check for updates

OPEN

Highly efficient TiO_2-supported Co–Cu catalysts for conversion of glycerol to 1,2-propanediol

Wongsaphat Mondach[1,2], Sarun Chanklang[1], Pooripong Somchuea[1], Thongthai Witoon[1,2,3], Metta Chareonpanich[1,2,3], Kajornsak Faungnawakij[4], Hiesang Sohn[5] & Anusorn Seubsai[1,2,3]✉

Glycerol is a low-cost byproduct of the biodiesel manufacturing process, which can be used to synthesize various value-added chemicals. Among them, 1,2-propanediol (1,2-PDO) is of great interest because it can be used as an intermediate and additive in many applications. This work investigated the hydrogenolysis of glycerol to 1,2-PDO over Co–Cu bimetallic catalysts supported on TiO_2 (denoted as CoCu/TiO_2) in aqueous media. The catalysts were prepared using the co-impregnation method and their physicochemical properties were characterized using several techniques. The addition of appropriate Cu increased the glycerol conversion and the 1,2-PDO yield. The highest 1,2-PDO yield was achieved over a 15Co0.5Cu/TiO_2 catalyst at 69.5% (glycerol conversion of 95.2% and 1,2-PDO selectivity of 73.0%). In the study on the effects of operating conditions, increasing the reaction temperature, initial pressure, and reaction time increased the glycerol conversion but decreased the selectivity to 1,2-PDO due to the degradation of formed 1,2-PDO to lower alcohols (1-propanol and 2-propanol). The reaction conditions to obtain the maximum 1,2-PDO yield were a catalyst-to-glycerol ratio of 0.028, a reaction temperature of 250 °C, an initial H_2 pressure of 4 MPa, and a reaction time of 4 h.

During the last decades, many research topics have focused on the development of renewable and sustainable energy resources owing primarily to the restricted availability of petroleum reserves and growing environmental concerns. Biomass and biomass-derived chemicals have attracted attention because as renewable sources, they can replace petroleum-derived fuels for sustainable development. Biodiesel is one of the most widely used renewable fuels, which can be used to replace conventional petroleum-based diesel directly for both stationary and mobile applications. In biodiesel production via transesterification of triglycerides in fat or oil, approximately 10% of crude glycerol is produced as a by-product[1]. Furthermore, the rapid expansion of biodiesel production has led to a rapid increase of byproduct glycerol and a decrease in its price. Therefore, the procedure for generating high value-added products from glycerol has received considerable attention and will substantially improve the economic viability of biodiesel production.

A variety of valorizations of glycerol, such as selective oxidation, hydrogenolysis, dehydration, transesterification, reforming, and condensation over heterogeneous catalysts have been reported for converting glycerol into valuable products[1–5]. Among the various possibilities of glycerol valorization, the catalytic hydrogenolysis of glycerol to 1,2-propanediol (1,2-PDO) has been one of the attractive alternatives because 1,2-PDO is a non-toxic chemical and is widely used as an intermediate and additive in many applications such as polyester resins, anti-freezing, engine cooling, paints, cosmetics, pharmaceuticals, and foods[6–8]. Currently, 1,2-PDO is produced mainly via the selective oxidation of petroleum-derived propylene to propylene oxide followed by hydrolysis[9]. However, the fluctuation in petroleum cost and increasing environmental concern have severely affected the production of 1,2-PDO via petroleum-derivatives. On the other hand, 1,2-PDO is produced using acid-catalyzed dehydration of the primary hydroxy group of glycerol to generate acetol, followed by hydrogenation over a catalyst. The latter process is more environmentally sustainable.

[1]Department of Chemical Engineering, Faculty of Engineering, Kasetsart University, Bangkok 10900, Thailand. [2]Center of Excellence on Petrochemical and Materials Technology, Kasetsart University, Bangkok 10900, Thailand. [3]Research Network of NANOTEC–KU on NanoCatalysts and NanoMaterials for Sustainable Energy and Environment, Kasetsart University, Bangkok 10900, Thailand. [4]Nanomaterials for Energy and Catalysis Laboratory, National Nanotechnology Center (NANOTEC), National Science and Technology Development Agency (NSTDA), Klong Laung, Pathumthani 12120, Thailand. [5]Department of Chemical Engineering, Kwangwoon University, Seoul 01897, Korea. ✉email: fengasn@ku.ac.th

Generally, hydrogenolysis is a class of reduction reaction that involves cleavage of the C–O bond in an organic compound with the simultaneous addition of a hydrogen atom to the resulting molecular fragments[8]. Specifically, the hydrogenolysis of glycerol to propanediol preferentially occurs over a bifunctional solid catalyst in either the vapor phase or the liquid phase of the reactants (glycerol and hydrogen). In other words, the catalyst for the hydrogenolysis of glycerol to 1,2-PDO must be bifunctional, with the first function being the dehydration at one of the primary hydroxyl groups of glycerol to hydroxy acetone (HA) and the second the hydrogenation of HA to 1,2-PDO as the product[10]. The catalysts shown to be active for the hydrogenolysis of glycerol to 1,2-PDO can be divided into two groups: (1) noble metal catalysts (such as Pt, Ru, Rh, Pd, and Re) are highly active in the activation of the hydrogen molecule; nevertheless, they often promote excessive cleavage of C–C bonds[11] and more importantly, they are expensive; (2) transition metal catalysts (such as Cu, Ni, and Co) have been intensively investigated in the hydrogenolysis of glycerol because they are inexpensive and highly resistant to catalyst poisoning. Among those various active metal catalysts, Co-based catalysts are interesting for an oxidation–reduction reaction, because they exhibit very low C–C bond cleavage but high activity for the selective catalytic hydrogenation of alkenes, aldehydes, and ketones[12]. These catalytic properties are beneficial for the hydrogenolysis of glycerol to propanediols. Nevertheless, only a few reports on Co-based catalysts have been reported in the hydrogenolysis of glycerol. For example, Gou et al. studied bi-functional Co/MgO catalysts, where the interaction between Co species and MgO was adjusted by the temperature of calcination for the glycerol hydrogenolysis to 1,2-PDO at 473 K, 2.0 MPa, and 9 h. They found that calcination at 873 K improved the interaction between Co_3O_4 and MgO, resulting in the prevention of aggregation of Co particles in the catalyst under extreme conditions. Their optimal glycerol conversion was 44.8% with 42.2% selectivity of 1,2-PDO[13]. Rekha et al. reported on a series of Co-ZnO catalysts prepared using the co-precipitation method and varying the Co-to-Zn ratio for the hydrogenolysis of glycerol to 1,2-PDO. The activity of the catalysts depended on the weight ratio of Co and ZnO and the maximum catalytic activity was obtained with a 50:50 weight ratio of Co-to-ZnO, with 70% glycerol conversion and 80% selectivity of 1,2-PDO[14].

The hydrogenolysis of glycerol also preferentially requires acidic sites from the catalysts because acidic sites can promote the dehydration of glycerol to HA, which is subsequently transformed to 1,2-PDO via hydrogenation[11,13,14]. In this manner, a catalyst support is commonly used to provide catalyst acidity. Thus, the selection of the catalyst support in the hydrogenolysis of glycerol to 1,2-PDO is also crucial. Various catalyst supports have been widely studied for the hydrogenolysis of glycerol, such as Al_2O_3, SiO_2, ZnO, TiO_2, and zeolite. Nevertheless, little research has been reported on the use of TiO_2 as an acidic support for the hydrogenolysis of glycerol. For example, Feng et al. studied the effect of support for the hydrogenolysis of glycerol. They found that the TiO_2 support had the smallest metal particle sites, resulting in the highest activity in the hydrogenolysis of glycerol. The maximum glycerol conversion was 90.1% with 20.6% selectivity of 1,2-PDO[15]. Salazar et al. reported that the 2.5Ru-2.5Cu/TiO_2 catalyst had the best performance of the hydrogenolysis of glycerol to 1,2-PDO because TiO_2 produced the smallest and most stable Ru particles, obtaining the highest yield of 1,2-PDO at 6.9% with 10% glycerol conversion and 69% selectivity of 1,2-PDO[16].

In the current study, we report for the first time the synthesis of bimetallic catalysts of Co and Cu supported on TiO_2 and their use for the hydrogenolysis of glycerol to 1,2-PDO. The characterization of the catalysts was also be studied to determine the chemical-physical properties, which were used to correlate with catalyst performance. Furthermore, the effect of the operating conditions—catalyst-to-glycerol ratio, reaction temperature, initial reaction pressure, and reaction time—was investigated for the hydrogenolysis of glycerol. Finally, the reusability of the catalyst was studied to determine catalyst stability after use for several cycles.

Materials and methods

Preparation of catalysts. The TiO_2 (21 nm primary particle size (TEM), ≥ 99.5% trace metals, Sigma-Aldrich) was used as a catalyst support. The CoCu/TiO_2 catalysts were prepared using the co-impregnation method. Aqueous solutions of $Co(NO_3)_2$•$6H_2O$ (2 M, 98%, QReC) and $Cu(NO_3)_2$•$3H_2O$ (1 M, 99%, Ajax) were used as the precursors for Co and Cu, respectively. The amount of Co was kept at 15 weight percent (wt%) but the amounts of Cu were varied at 0, 0.25, 0.5, 1.0, or 2.0 wt.%. The predetermined amount of the Co and Cu solutions was loaded on the TiO_2 support. Then, each mixture solution was continuously stirred at room temperature for 1 h. The mixture was then dried in a hot-air oven at 100 °C for 12 h and calcined in an air furnace at 500 °C and a heating rate of 5 °C min^{-1} for 4 h to obtain xCoyCu/TiO_2 catalysts (where x = 15 wt% of Co and y = 0, 0.25, 0.5, 1 or 2 wt% of Cu, respectively).

Catalyst activity studies. The activity of each prepared catalyst was evaluated in a teflon-lined stainless-steel autoclave (Parr 4848, actual volume = 200 mL), which was equipped with an electromagnetic stirrer and a temperature controller unit. Before the reaction, each catalyst was reduced using H_2 at a flow rate of 50 mL min^{-1} at 350 °C for 1 h in a plug flow reactor. Then, the catalyst was transferred to the teflon-lined stainless-steel reactor. Subsequently, glycerol (10 mL, 99.5%, QReC) and deionized water (10 mL) were rapidly introduced into the reactor to prevent the reduced catalyst from contact with air. Afterward, the reactor was sealed and purged three times with pure H_2 (99.999%, Air liquide) to eliminate any air. The reactor was pressurized to the desired H_2 pressure (2, 4, or 6 MPa) and the stirring speed was set at 800 rounds per minute (rpm). Then, the reactor system was heated to the desired reaction temperature (210, 230, 250, or 270 °C). After the reaction, the reactor was cooled to room temperature and the pressure was released to ambient conditions. A small amount of the liquid products (5.0 mL) was then sampled using a syringe filter (nylon 0.45 µm, CNW Technologies) for product analysis using gas chromatography (Shimadzu, GC-14A), equipped with a DB-WAX capillary column (30 m long, 0.53 mm inner diameter, and 1 µm thickness) and a flame ionization detector. The detected liquid products were 1,2-propanediol (1,2-PDO), 1,3-propanediol (1,3-PDO), 1-propanol (1-PO), 2-propanol (2-PO), HA, and

ethylene glycol (EG). For the quantification of each product, the pure chemical was purchased and a standard calibration curve with four concentration points and a coefficient of determination (R^2) > 0.99 was made using GC. The activity of the catalysts was presented in terms of glycerol conversion (%), product selectivity (%), and product yield (%) as shown in Eqs. (1), (2), and (3), respectively:

$$\text{Glycerol conversion (\%)} = \frac{n_{\text{in}}^{\text{gly}} - n_{\text{out}}^{\text{gly}}}{n_{\text{in}}^{\text{gly}}} \times 100 \quad (1)$$

$$\text{Product selectivity (\%)} = \frac{n_p}{n_{\text{in}}^{\text{gly}} - n_{\text{out}}^{\text{gly}}} \times \frac{Z_p}{Z_{\text{gly}}} \times 100 \quad (2)$$

$$\text{Product yield (\%)} = \frac{\text{\% Glycerol conversion} \times \text{\%Product selectivity}}{100} \quad (3)$$

where $n_{\text{in}}^{\text{gly}}$ is the molar amount of glycerol before the reaction (blank), $n_{\text{out}}^{\text{gly}}$ is the molar amount of unreacted glycerol after the reaction, and n_p is the molar amount of desired product. Z_p and Z_{gly} are the number of carbon atoms of the desired product and glycerol, respectively. Note that, for the catalytic activity data, "others" refers to 2-PO, HA, and other unquantified products including gaseous products (e.g. propane and ethane).

For the reusability test of the catalyst, after the first cycle of the reaction, the catalyst was separated from the liquid products using a centrifuge at 8000 rpm for 15 min. Then, the catalyst was washed three times with DI water, dried overnight in the hot-air oven, and reduced using the H_2 flow as described previously before the new cycle of the reaction.

Characterization of catalysts. The crystalline phases and the average metal crystallite sizes of the catalysts were analyzed using powder x-ray diffraction (XRD, JEOL JDX-3530 and Philips X-Pert) with Cu-Kα radiation at 45 kV and 40 mA at an angle (2θ) range of 10–80°. A step size of 0.02° and a step time of 0.5 s were used for the measurements.

The particle size distribution and the elemental composition mapping of the samples were analyzed using transmission electron microscopy with energy-dispersive X-ray spectroscopy (TEM with EDX: JEM-2100). After reduction with H_2 at 350 °C, the samples were suspended in ethanol solvent, dropped on carbon film coated on Cu TEM grids, and dried in a chamber filled with N_2 at room temperature before the analysis.

The surface area, pore volume, and average pore size of the catalysts were determined using an N_2-physisorption analyzer (Brunauer–Emmett–Teller (BET): 3Flex Physisorption Micromeritics) at − 196 °C. Each catalyst was pretreated at 300 °C for 24 h in the system of the N_2-physisorption analyzer before measurement. For each catalyst, the BET surface area was determined in a relative pressure (P/P^0) range of 0.05–0.30; the total pore volume was determined at P/P^0 of 0.995, and the pore size was computed using the Barrett-Joyner-Halenda method.

The elemental composition of the catalysts was determined using inductively coupled plasma-optical emission spectrometry (ICP-OES). Before the ICP-OES measurements, the solid samples were dissolved in hydrochloric acid solution.

The electronic states of cobalt (Co 2p) and copper (Cu 2p) for the samples were analyzed using x-ray photoelectron spectrometry (XPS; Kratos Axis Ultra DLD), using Al K_α for the x-ray source.

The reducibility of the catalysts was analyzed using H_2-Temperature-Programmed Reduction (H_2-TPR, Micromeritics AutoChem II). Before the H_2-TPR experiments, each catalyst (0.1 g) was pretreated at 120 °C and a heating rate of 5 °C min^{-1} under an He flow (50 mL min^{-1}). Then, it was cooled to 50 °C and then heated to 900 °C at a heating rate of 10 °C min^{-1} under a flow of 10% H_2 in Ar. The H_2 consumed during the reduction was continuously monitored using a thermal conductivity detector (TCD).

The acidity of the catalysts was analyzed using NH_3 temperature-programmed desorption (NH_3-TPD, Micromeritics AutoChem II). Before the NH_3-TPD experiments, each catalyst (0.1 g) was pretreated using the same method as the pretreatment for the H_2-TPR experiments. After the catalyst had cooled to 50 °C, it was exposed to 0.2% NH_3 in He for 1 h followed by purging with He for 1 h. Finally, the NH_3-TPD measurement was carried out from 50 to 900 °C at a heating rate of 10 °C min^{-1}. The NH_3-desorption was continuously monitored using a TCD. Note that all gas flow rates were 25 mL min^{-1} for gas/gas mixture measurements.

The surface morphology of the catalysts was analyzed using scanning electron microscopy (SEM; JEOL, JSM7600 F). Samples were imaged at a working distance of 4.0 mm and an acceleration voltage of 1.0 kV.

Results and discussion

Catalyst characterization. *The crystallization analysis of catalysts by XRD.* The XRD patterns of 15Co/TiO_2, 15Co0.5Cu/TiO_2, 15Co1Cu/TiO_2, and 0.5Cu/TiO_2 in the 2θ range from 10° to 80° are shown in Fig. 1. Note that the XRD measurement of all catalysts was carried out after the H_2 reduction. As observed, the diffraction peaks of TiO_2 with both anatase (2θ = 25.3°, 37.9°, 48.0°, 53.9°, and 62.6°)[17] and rutile (2θ = 27.4°, 36.1°, 36.9°, 38.5°, and 41.2°)[16] structures were observed in every catalyst, and all the XRD peaks of TiO_2 were almost identical. This suggested that the loading of Co and Cu metal had not affected the crystallinity of the TiO_2. In the XRD profiles of 15Co/TiO_2, 15Co0.5Cu/TiO_2, and 15Co1Cu/TiO_2, only one clear diffraction peak of metallic Co at 2θ = 44.3°[18] was observed; other diffraction peaks indicating the metallic Co (e.g. 2θ = 36.9° and 62.6°) were overlapped with the diffraction peaks of the TiO_2. For the Cu-containing catalysts, no diffraction peak of

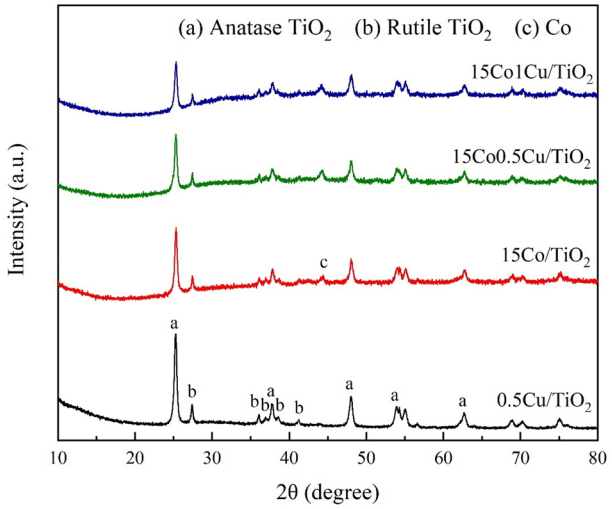

Figure 1. XRD patterns of (**a**) 0.5Cu/TiO_2, (**b**) 15Co/TiO_2, (**c**) 15Co0.5Cu/TiO_2, and (**d**) 15Co1Cu/TiO_2.

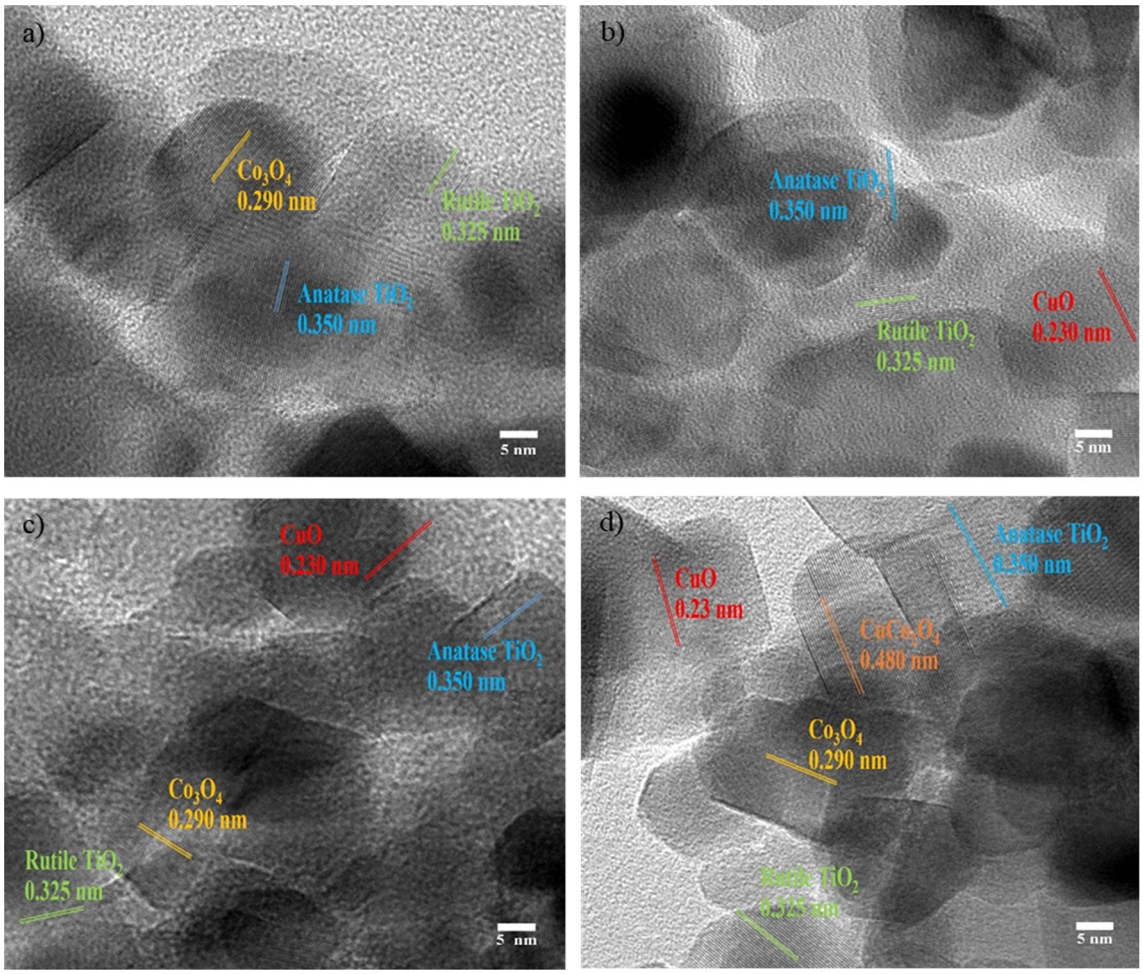

Figure 2. TEM images of (**a**) 15Co/TiO_2, (**b**) 0.5Cu/TiO_2, (**c**) 15Co0.5Cu/TiO_2, and (**d**) 15Co1Cu/TiO_2.

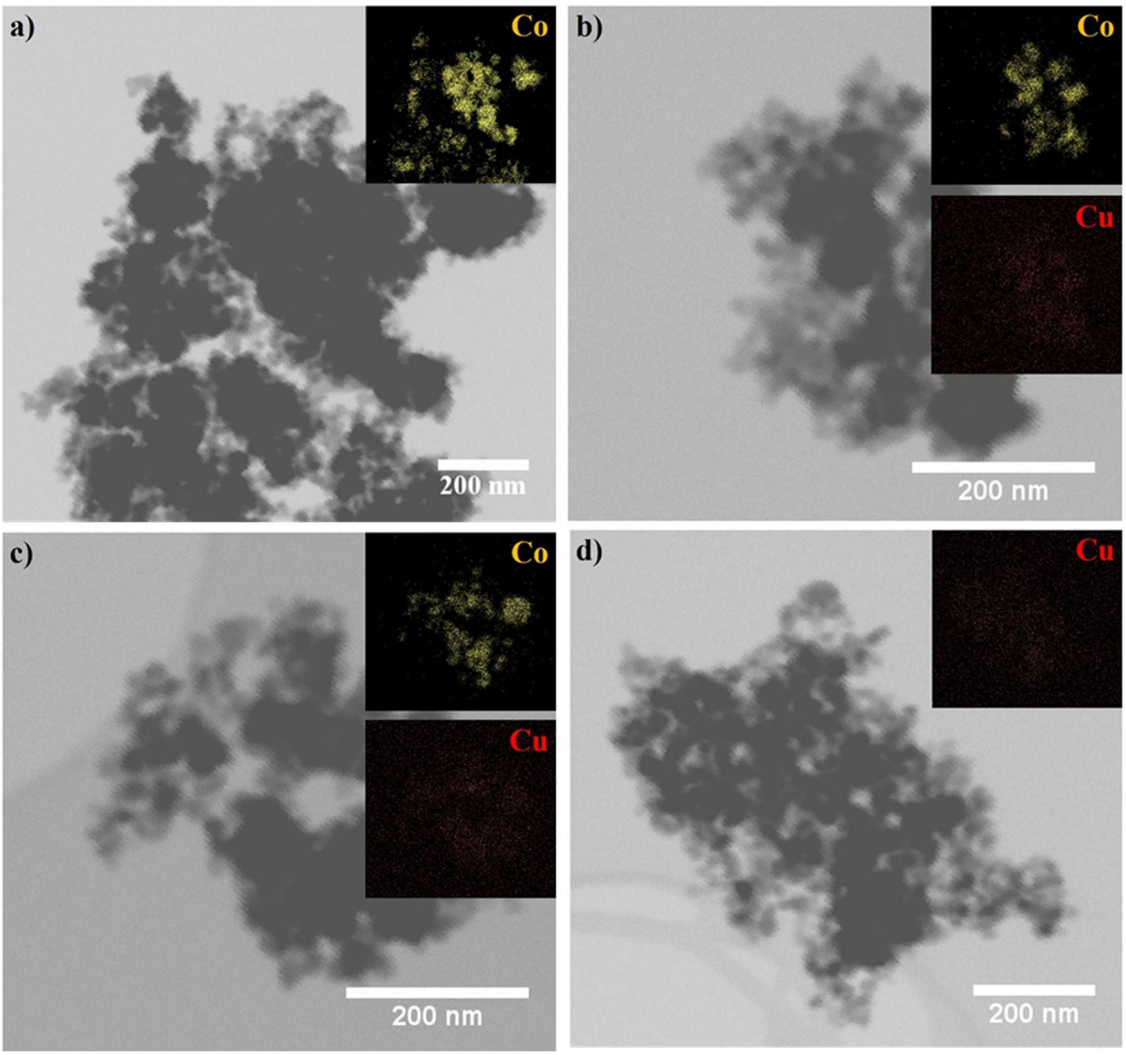

Figure 3. TEM with EDX images of (**a**) 15Co/TiO_2, (**b**) 15Co0.5Cu/TiO_2, (**c**) 15Co1Cu/TiO_2, and (**d**) 0.5Cu/TiO_2.

Cu species was observed, possibly because the amount of Cu loading was small (< 2 wt%) and the crystal size of the Cu species was smaller than the size limit detection of the instrument (< 2.5 nm).

The morphological analysis of catalysts by TEM. The structural morphologies of 15Co/TiO_2, 15Co0.5Cu/TiO_2, 15Co1Cu/TiO_2, and 0.5Cu/TiO_2 were characterized using TEM, as shown in Fig. 2. Note that the catalysts were exposed to air before imaging using TEM because of this limitation during the sample preparation for the TEM experiment. As observed, the oxides of Co and/or Cu were distributed throughout the TiO_2 support. Every sample had a lattice d-spacing of 0.325 nm and 0.350 nm, specifying the crystal planes of the TiO_2-rutile phase [1 1 0] and the TiO_2-anatase phase [1 0 1], respectively[19]. Figure 2a illustrates the 15Co/TiO_2 lattice d-spacing of 0.290 nm, indicating the crystal plane of Co_3O_4 [2 2 0]. Figure 2b illustrates the 0.5Cu/TiO_2 lattice d-spacing of 0.230 nm, corresponding to the crystal plane of CuO [1 1 1][20]. For the bimetallic catalysts in Figs. 2c and 2d, both crystal planes of Co_3O_4 and CuO were observed in each bimetallic catalyst. Additionally, 15Co1Cu/TiO_2 had lattice d-spacing of 0.480 nm, assigned to the $CuCO_2O_4$ phase[21]. Furthermore, the elemental distributions on the surface of 15Co/TiO_2, 15Co0.5Cu/TiO_2, 15Co1Cu/TiO_2, and 0.5Cu/TiO_2 were analyzed using TEM with EDX-mapping, as shown in Fig. 3. The cobalt and copper species on the TiO_2 support correlated to the bright yellow and red spots on the EDX-mapping images, respectively. As seen, both metal species were uniformly distributed on the surface of the support. Based on the XRD results, the Cu species in 0.5Cu/TiO_2, 15Co0.5Cu/TiO_2, and 15Co1Cu/TiO_2, and the $CuCO_2O_4$ phase in 15Co1Cu/TiO_2 were not observed. These results from TEM and TEM with EDX-mapping confirmed that the Cu and $CuCo_2O_4$ species were present in the catalysts.

The textural property analysis by N_2-physisorption. The textural properties (BET surface area, pore size diameter, and pore volume) of TiO_2, 15Co/TiO_2, 15Co0.5Cu/TiO_2, 15Co1Cu/TiO_2, and 0.5Cu/TiO_2 were determined using N_2-sorption analysis, as shown in Table 1. Furthermore, to evaluate the N_2 adsorption–desorption isotherm of each catalyst, the plot of the amount of N_2 adsorbed and desorbed for each catalyst versus the relative

Catalysts	Metal composition (%)		BET surface area ($m^2 g^{-1}$)	Pore volume ($cm^3 g^{-1}$)	Average pore diameter (nm)
	Co	Cu			
TiO_2	–	–	50.5	0.69	41.5
$15Co/TiO_2$	14.45	–	41.8	0.31	40.0
$15Co0.5Cu/TiO_2$	15.44	0.62	37.3	0.28	50.5
$15Co1Cu/TiO_2$	14.83	1.22	34.1	0.29	49.6
$0.5Cu/TiO_2$	–	0.44	48.9	0.41	39.4

Table 1. Textural properties and elemental composition of TiO_2, $15Co/TiO_2$, $15Co0.5Cu/TiO_2$, $15Co1Cu/TiO_2$, and $0.5Cu/TiO_2$.

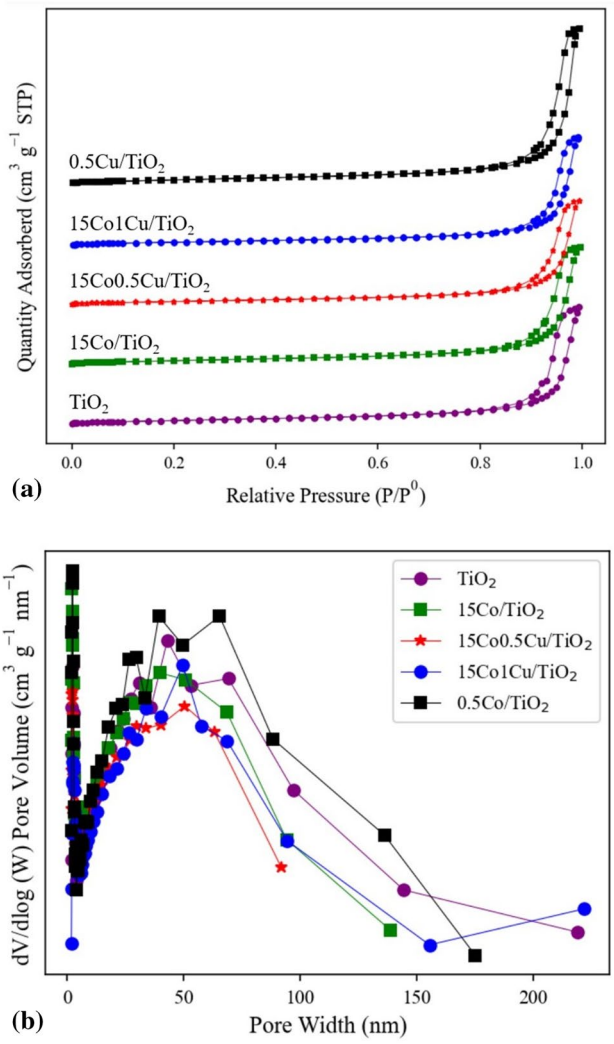

Figure 4. (**a**) N_2 adsorption–desorption isotherms and (**b**) pore size distribution of TiO_2, $15Co/TiO_2$, $15Co0.5Cu/TiO_2$, $15Co1Cu/TiO_2$, and $0.5Cu/TiO_2$.

pressure (P/P^0) is shown in Fig. 4a. The plot of the pore size distribution of each catalyst is shown in Fig. 4b. Note that, before the BET measurement, the pure TiO_2 was treated using the same procedure as the catalyst preparation, except for adding the active metals. In Table 1, the pure TiO_2 support had the greatest BET surface area ($50.5 m^2 g^{-1}$) with the largest pore volume ($0.69 cm^3 g^{-1}$). After Co and/or Cu were impregnated onto the TiO_2 support, the surface areas became smaller than those of the pure TiO_2, and the pore volumes and average pore size diameters were similarly in the ranges 0.29–0.41 $cm^3 g^{-1}$ and 39.4–50.5 nm, respectively. Additionally, the

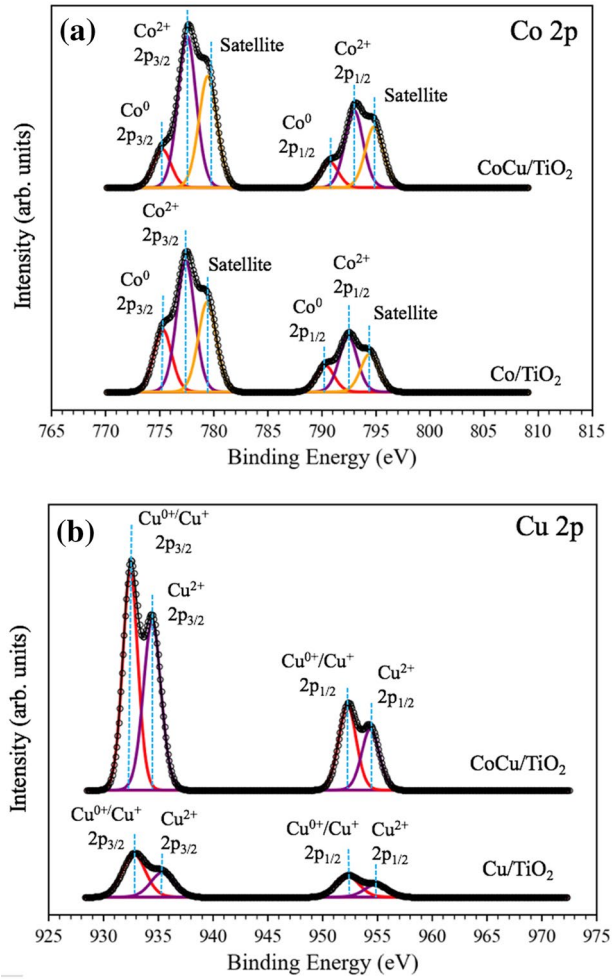

Figure 5. XPS spectra of (**a**) Co 2p of Co/TiO_2 and $CoCu/TiO_2$ and (**b**) Cu 2p of Cu/TiO_2 and $CoCu/TiO_2$.

greater the amount of loaded active metals, the lower the BET surface area, probably because the active metals filled the pores of the TiO_2 support during the catalyst preparation.

The plots in Fig. 4a describe the adsorption–desorption behavior of N_2 onto the catalyst surface. According to the IUPAC classification, all the catalysts were classified into the type IV isotherm, identifying them as a mesopore material consisting of multilayer adsorption followed by pore condensation[22]. A hysteresis loop can be seen above P/P^0 values of 0.8 for every catalyst and it can be classified as type H3 hysteresis, revealing the capillary condensation of mesoporous materials[23]. For the pore size distribution curve shown in Fig. 4b, the peaks of all samples were very close to each other, approximately 50 nm.

The elemental composition analysis by ICP-OES. The elemental compositions of $15Co/TiO_2$, $15Co0.5Cu/TiO_2$, $15Co1Cu/TiO_2$, and $0.5Cu/TiO_2$ were determined using ICP-OES, as shown in Table 1. The results indicated that the actual amount of cobalt and/or copper in each catalyst was close to the theoretical value.

The oxidation states analysis of catalysts by XPS. The surface chemical states of the catalysts were determined using XPS, as shown in Fig. 5. For the Co spectra (Fig. 5a.), the deconvoluted peaks at 775.3, 777.4, and 779.4 eV in the orbital $2p_{3/2}$ position corresponded to the metallic Co^0, Co^{2+}, and satellites, respectively[24]. The binding energy (B.E.) value between each spin–orbit separation of Co $2p_{3/2}$ and Co $2p_{1/2}$ was consistent at 15 eV, which is characteristic of Co_3O_4 spinel[25]. The greatest area of the deconvoluted peak at 777.4 eV indicated that the Co^{2+} species represented the greatest amount among all the cobalt species[26]. For the Cu spectra (Fig. 5b), the deconvoluted peaks at 934.6 eV and 954.6 eV corresponded to Cu $2p_{3/2}$ and Cu $2p_{1/2}$, respectively. The splitting energy of 20 eV indicated the formation of Cu^{2+}[27]. Furthermore, the deconvoluted peak at 932.5 eV in the orbital Cu $2p_{3/2}$ position could be assigned to Cu^0 or Cu^+ because the range of the B.E.s for Cu^0 and Cu^+ are overlapped[26]. After adding the Cu to Co/TiO_2, a positive shift for the B.E. of Cu on $CoCu/TiO_2$ was observed. This phenomenon was similarly observed in other Co–Cu catalysts for methanol decomposition to hydrogen production[26] and direct synthesis of ethanol and higher alcohols from syngas[28]. This indicates that copper loses electrons and variation of copper chemical states in the bimetallic Co–Cu catalysts[26]. In other words, an electronic interaction occurs between the Co and Cu species over the TiO_2 support.

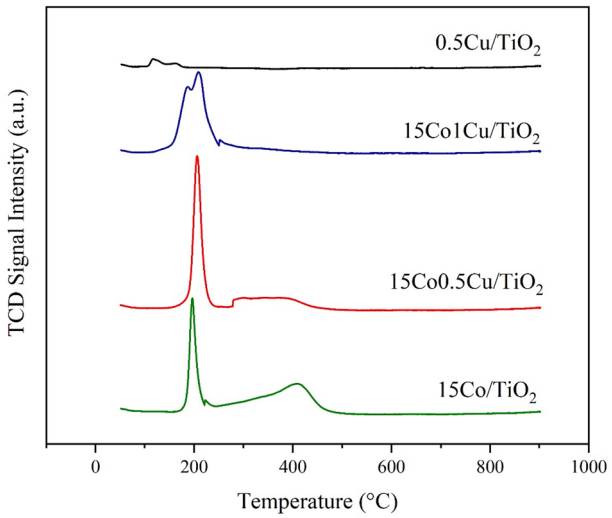

Figure 6. H_2-TPR profiles of 15Co/TiO_2, 15Co0.5Cu/TiO_2, 15Co1Cu/TiO_2, and 0.5Cu/TiO_2.

Catalysts	Acid amount (mmol of NH_3/g of catalyst)			
	Weak acid	Moderate acid	Strong acid	Total acid
TiO_2	0.23	0.10	0.15	0.48
15Co/TiO_2	0.08	0.11	0.06	0.25
15Co0.5Cu/TiO_2	0.12	0.10	0.06	0.28
0.5Cu/TiO_2	0.08	0.04	0.07	0.19

Table 2. Acidity of TiO_2, 15Co/TiO_2, 15Co0.5Cu/TiO_2, and 0.5Cu/TiO_2.

The reducibility analysis of catalysts by H_2-TPR. The reducibility of 15Co/TiO_2, 15Co0.5Cu/TiO_2, 15Co1Cu/TiO_2, and 0.5Cu/TiO_2 was characterized using H_2-TPR, as shown in Fig. 6. The H_2-TPR profile of the catalysts can be used to identify the species of metal on the surface and the nature of the active site of the catalysts. For the monometallic catalysts, the 15Co/TiO_2 had two reduction peaks, with one sharp peak at 200 °C and one broad reduction peak between 240 to 500 °C, assigned to the reductions of Co_3O_4 to CoO and CoO to Co, respectively[25]. The TPR profile of 0.5Cu/TiO_2 had a reduction peak at 115 °C with a shoulder peak at 160 °C, corresponding to the reduction of Cu_2O and CuO to Cu, respectively[29]. For the bimetallic catalysts, the TPR profile of 15Co0.5Cu/TiO_2 had an overlapped peak at a lower temperature (205 °C) involved with the reduction of Co_3O_4 to CoO, CuO to Cu, and $Cu_xCo_{3-x}O_4$ to Cu and Co[30], and a relatively large broad reduction peak at higher temperature (approximately 280–500 °C), assigned to the reduction of CoO to Co[31]. Interestingly, 15Co1Cu/TiO_2 had an overlapped reduction peak around 100–250 °C with a relatively small broad peak around 250–300 °C. This can be explained by 15Co1Cu/TiO_2, with the main peak and a shoulder peak around 100–250 °C being attributed to a complicated reduction of the oxides of Cu and Co to Cu and Co, suggesting that the Cu- and Co-species particles were in close contact, which led to an occurrence of a spillover mechanism during the reduction of the Co–Cu catalysts[32]. In other words, because of the close contact of the Cu- and Co-species particles, the adsorbed atomic hydrogen could transfer from Cu^0 to Co oxide species and encouraged reduction to Co^0.

The acidity analysis of the catalysts by NH_3-TPD. The acidity of 15Co/TiO_2, 15Co0.5Cu/TiO_2, and 0.5Cu/TiO_2 was determined using NH_3-TPD, as shown in Table 2. The acid sites were calculated from the peak areas of NH_3 desorption signals in different temperature ranges, which can be defined as weak acid sites (< 300 °C), medium acid sites (300–500 °C), and strong acid sites (> 500 °C)[32]. From Table 2, the TiO_2 support had the highest number of total acid sites. After the metals were impregnated, the total acid sites of catalysts decreased, which was attributed to the occupation of acid sites by metal species[11]. For the bimetallic catalyst, the addition of Cu to Co/TiO_2 enhanced the formation of acid sites due to the formation of $CuCo_2O_4$ species[32] (as deduced from TEM) and the synergistic interaction of these metals with the TiO_2 support[11].

The activity of catalysts for hydrogenolysis of glycerol to 1,2-PDO. The prepared catalysts were investigated for hydrogenolysis of glycerol to 1,2-PDO at 230 °C with a hydrogen pressure of 4 MPa for 4 h. The results in terms of glycerol conversion, selectivity, and 1,2-PDO yield are summarized in Table 3. The 15Co/TiO_2 monometallic catalyst achieved 46.2% of glycerol conversion and 81.1% of 1,2-PDO selectivity, giving a 1,2-PDO yield of 37.5%; meanwhile, the 0.5Cu/TiO_2 monometallic catalyst had a very low 1,2-PDO yield at 1.0%. Increasing the Cu loading on Co/TiO_2 increased the 1,2-PDO formation, yielding the maximum 1,2-PDO

Catalyst	Conversion (%)	Selectivity (%)					1,2-PDO yield (%)
		1,2-PDO	1,3-PDO	EG	1-PO	Others	
15Co/TiO_2	46.2	81.1	1.6	7.7	4.7	0.8	37.5
15Co0.25Cu/TiO_2	47.4	84.1	1.3	5.8	5.3	1.0	39.9
15Co0.5Cu/TiO_2	60.2	86.0	1.3	7.0	3.6	0.8	51.8
15Co1Cu/TiO_2	44.5	90.5	0.9	3.5	3.2	1.1	40.3
15Co2Cu/TiO_2	30.3	85.1	1.0	1.7	8.7	2.4	25.8
0.5Cu/TiO_2	2.3	41.6	14.8	2.0	22.2	17.8	1.0

Table 3. Catalytic activity for hydrogenolysis of glycerol over CoCu/TiO_2. Reaction conditions: 0.5 g catalyst, 230 °C, 4 MPa, and 4 h.

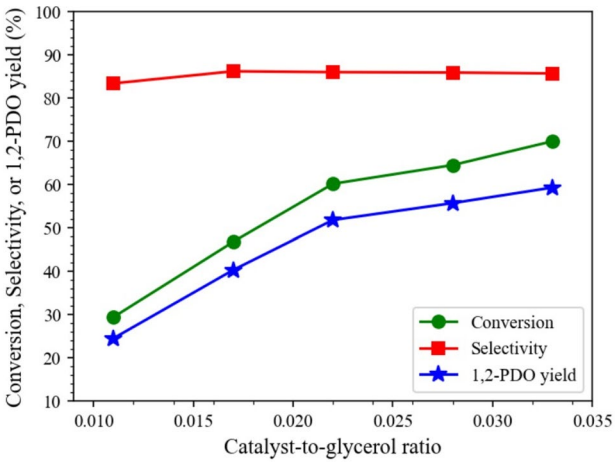

Figure 7. Effect of catalyst-to-glycerol ratio on hydrogenolysis of glycerol, with reaction conditions: 230 °C, 4 MPa, and 4 h, and glycerol solution amount fixed at 20 mL (22.6 g).

at 51.8% with 60.2% glycerol conversion and 86.0% of 1,2-PDO selectivity when the Cu loading was 0.5 wt%. This was because i) there was a synergistic catalytic effect between the Co and Cu that occurred between the interfaces of these metal particles; ii) there was an increase in acid sites[33], especially the weak acid site when the Cu was added to Co/TiO_2 (as indicated in the NH_3-TPD results in Table 2) that can favor the activation of the C—O bond from glycerol to HA during the dehydration step[34] so that the glycerol conversion increased; and iii) the presence of multiple Co sites (as indicated in the results of XPS in Fig. 5 and H2-TPR in Fig. 6) promoted the overall hydrogenolysis of glycerol to 1,2-PDO[21,32].

Increasing the Cu loading on Co/TiO_2 from 0.5 to 2 wt% decreased the performance of the catalysts, probably because the excess amount of Cu over the surface (as indicated by the H_2-TPR results in Fig. 6) could reduce the number of interfaces between Co and Cu. In addition, the catalyst's pores could have been blocked by the high metal loadings[35] (as indicated by the BET results in Table 1).

Effect of operating conditions. *Catalyst-to-glycerol ratio.* The effect of the glycerol-to-catalyst ratio on the hydrogenolysis of glycerol over 15Co0.5Cu/TiO_2 is presented in Fig. 7. The catalyst-to-glycerol ratio (on a weight basis) was varied from 0.011 to 0.033. As observed, increasing the catalyst-to-glycerol ratio from 0.011 to 0.033 increased the glycerol conversion and the 1,2-PDO yield from 29.4% to 69.8% and 24.5% to 59.3%, respectively, because the number of active sites increased with the increasing catalyst-to-glycerol ratio [33,36]. It was also observed that the selectivity of 1,2-PDO did not change much in this range for the catalyst-to-glycerol ratio; the selectivity of 1,2-PDO was approximately 83–86%, implying that over hydrogenolysis of 1,2-PDO did not occur.

Reaction temperature. The effect was investigated of the reaction temperature on the activity of the hydrogenolysis of glycerol over 15Co0.5Cu/TiO_2 and the results are shown in Fig. 8. The increase in reaction temperature from 210 to 270 °C led to a large increase in the glycerol conversion from 21.9 to 99.6%. The selectivity toward 1,2-PDO gradually decreased from 90.0 to 51.5% and the maximum 1,2-PDO yield at 69.5% was obtained at 250 °C. The results indicated that the higher reaction temperature favored glycerol conversion but led to lower selectivity of 1,2-PDO due to the formation of 1-PO and 2-PO[11,13].

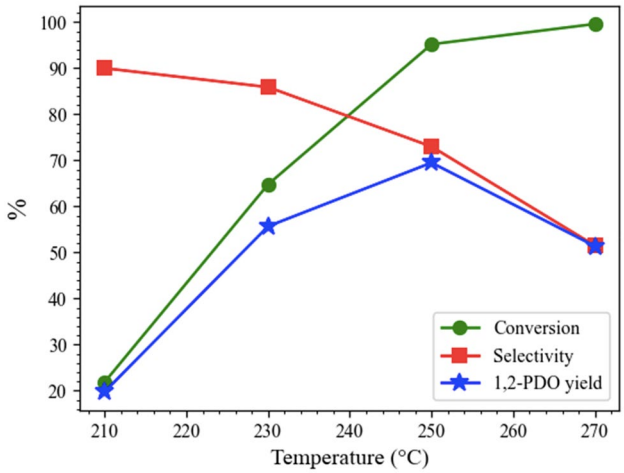

Figure 8. Effect of reaction temperature on hydrogenolysis of glycerol, with reaction conditions: catalyst-to-glycerol ratio of 0.028, 4 MPa, and 4 h, and glycerol solution amount fixed at 20 mL (22.6 g).

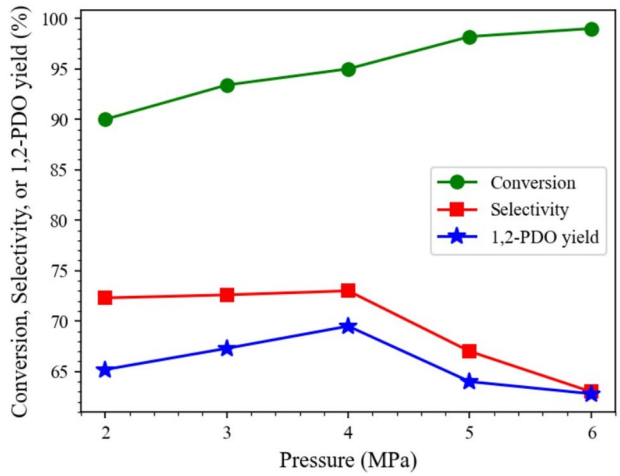

Figure 9. Effect of hydrogen pressure on hydrogenolysis of glycerol, with reaction conditions: 0.028 catalyst-to-glycerol ratio, 250 °C, and 4 h, and glycerol solution amount fixed at 20 mL (22.6 g).

Reaction pressure. The effect was examined of initial hydrogen pressure in the pressure range 2–6 MPa on the glycerol hydrogenolysis over 15Co0.5Cu/TiO_2 at 250 °C, as presented in Fig. 9. Increasing the initial pressure from 2 to 6 MPa resulted in an increased glycerol conversion from 90.2 to 99.8%, because the solubility of hydrogen into an aqueous solution was enhanced by the increased pressure[13]. The selectivity toward 1,2-PDO slightly increased from 72.3 to 73.0% and further sharply decreased to 63.0% at 6 MPa hydrogen pressure due to the degradation of 1,2-PDO to 1-PO and 2-PO[14]. Therefore, the optimal initial hydrogen pressure to obtain the maximum 1,2-PDO yield was 4 MPa for this catalyst.

Reaction time. The effect of reaction time on the glycerol hydrogenolysis over 15Co0.5Cu/TiO_2 was investigated at a catalyst-to-glycerol ratio of 0.028, a reaction temperature of 250 °C, and an initial hydrogen pressure of 4 MPa, as shown in Fig. 10. As seen, the glycerol conversion increased from 90.2 to 99.8% when the reaction time increased from 2 to 8 h. However, the selectivity of 1,2-PDO decreased from 72.3 to 63.0% with increasing reaction time, which also contributed to the degradation of formed 1,2-PDO to 1-PO[7]. Overall, the local optimal reactions to obtain the maximum 1,2-PDO yield (69.5%) was a catalyst-to-glycerol ratio of 0.028, a reaction temperature of 250 °C, an initial hydrogen pressure of 4 MPa, and a reaction time of 4 h for this catalyst.

Reusability test of 15Co0.5Cu/TiO_2. The reusability of the catalyst is an important factor that should be considered for commercial purposes. The reusability of 15Co0.5Cu/TiO_2 for the hydrogenolysis of glycerol over five cycles is shown in Fig. 11. As observed, the glycerol conversion and the 1,2-PDO yield decreased after each hydrogenolysis of glycerol reaction. After five cycles, the glycerol conversion and 1,2-PDO yields decreased from 95.2% and 69.5% to 52.5% and 29.3%, respectively, while 1,2-PDO selectivity gradually decreased from 73.0%

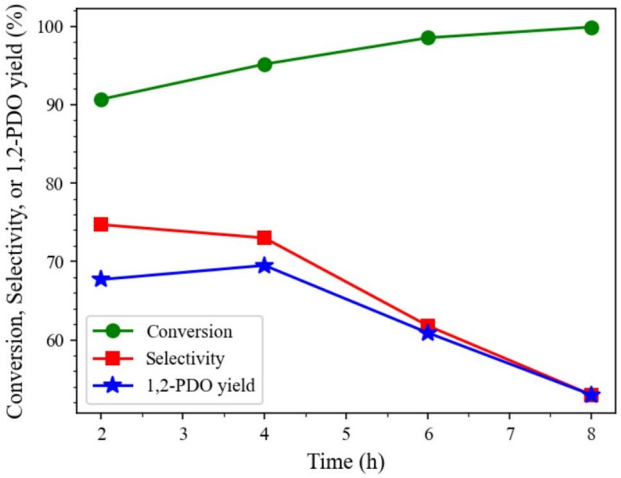

Figure 10. Effect of reaction time on hydrogenolysis of glycerol, with reaction conditions: 0.028 catalyst-to-glycerol ratio, 250 °C, and 4 MPa, and glycerol solution amount fixed at 20 ml (22.6 g).

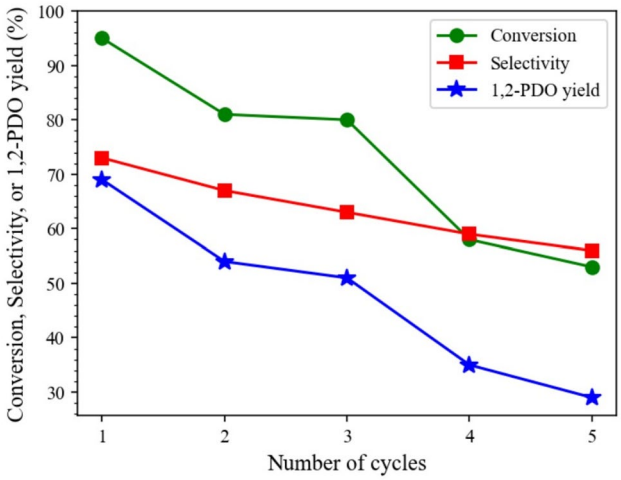

Figure 11. Reusability of 15Co0.5Cu/TiO_2 for hydrogenolysis of glycerol to 1,2-PDO, with reaction conditions: 0.028 catalyst-to-glycerol ratio, 250 °C, and 4 MPa, and glycerol solution amount fixed at 20 ml (22.6 g).

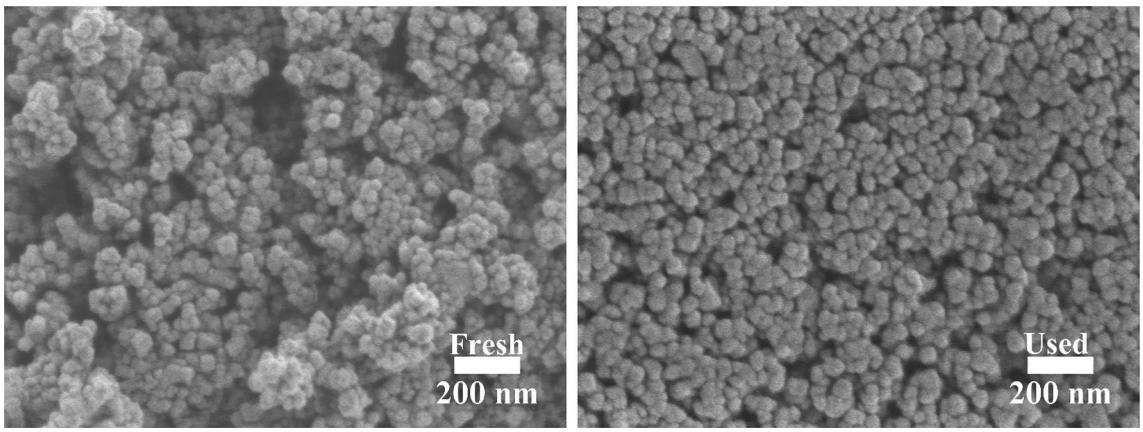

Figure 12. SEM images of fresh and used 15Co0.5Cu/TiO_2.

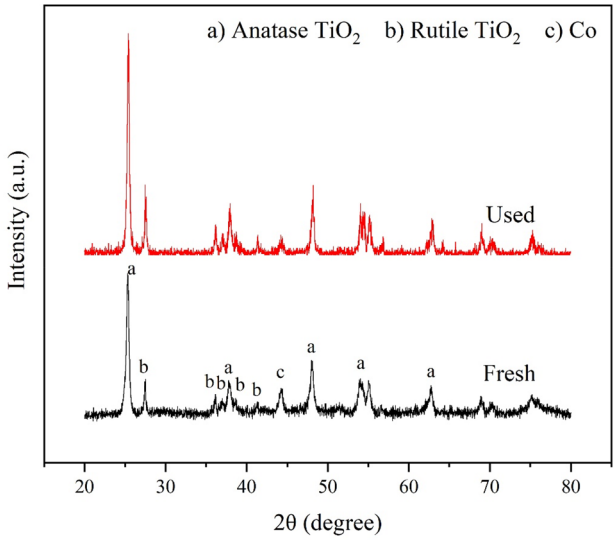

Figure 13. XRD pattern of fresh and used 15Co0.5Cu/TiO_2.

Catalyst	BET surface area ($m^2\ g^{-1}$)	Pore volume ($cm^3\ g^{-1}$)	Average pore diameter (nm)
Fresh 15Co0.5Cu/TiO_2	37.3	0.28	50.5
Used 15Co0.5Cu/TiO_2	37.7	0.33	65.5

Table 4. Textural properties of fresh and used 15Co0.5Cu/TiO_2.

Catalysts	Metal composition (%)	
	Co	Cu
Fresh 15Co0.5Cu/TiO_2	15.44	0.62
Used 15Co0.5Cu/TiO_2	11.10	0.77

Table 5. Elemental composition of fresh and used 15Co0.5Cu/TiO_2.

to 55.8%. The catalyst used for five cycles was further analyzed for its physicochemical properties using SEM, XRD, and N_2-physisorption, as shown in Figs. 12 and 13, and Table 4, respectively. Comparing the SEM images, N_2-physisorption results, and XRD pattern of the fresh and used catalysts, the surface morphology, the textural properties, and the crystalline properties were similar. In contrast, the analysis of the fresh catalyst and the used catalyst after five cycles using ICP-OES (see Table 5) showed that the amount of Co had substantially decreased in the used catalyst. Furthermore, the crude product of the hydrogenolysis of the glycerol reaction was analyzed using ICP-OES; it was found that the amounts of Co and Cu in the crude product were 374.5 and 0.2 ppm, respectively. These results indicated that gradual leaching, especially of Co, occurred during the reaction and the recycling process, leading to the gradual deactivation of the catalyst, similar to the results reported by Feng et al.[7] A further study in the prevention of the leaching is, therefore, needed.

Comparative activity of the catalysts for hydrogenolysis of glycerol to 1,2-PDO. From previous research, most catalysts were bifunctional, consisting of acidic sites and metallic sites, which are involved in the dehydration and hydrogenation steps, respectively. Figure 14 illustrates the comparative activity of bifunctional catalysts for the hydrogenolysis of glycerol to 1,2-PDO, with the detail of each catalyst shown in Table S1. High reaction temperatures around 170–250 °C are commonly used since the hydrogenolysis of glycerol is an endothermic reaction. In addition, high initial H_2 pressures around 1–6 MPa are preferred because they provide an extensive massive dispersion of H_2 and more H_2 is dissolved in the liquid phase, which is advantageous for the hydrogenolysis of glycerol. Comparing our catalyst performance with others, CoCu/TiO_2 was highly effective in the hydrogenolysis of glycerol to 1,2-PDO, achieving a maximum 1,2-PDO yield at 69.5% with 95.2% glycerol conversion in the current study. Catalysts providing a 1,2-PDO yield above 90% are shown in Fig. 14 include Cu–Zn-Mg–Al-O with the addition of NaOH[37], Cu@SiO_2 core–shell-catalysts with a Cu/Si atomic ratio of 2[38], and PdCu-KF/Al_2O_3[7]. Nevertheless, our catalyst can be easily prepared, the Cu and Co precursors are relatively

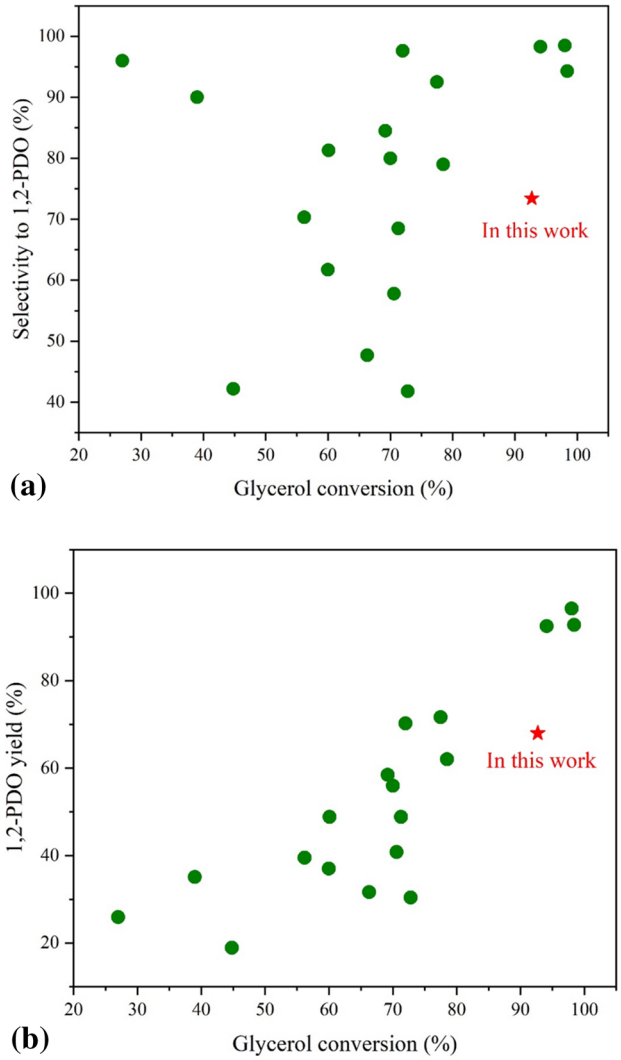

Figure 14. Comparative activity of Co- or Cu-based catalysts for hydrogenolysis of glycerol (**a**) selectivity to 1,2-PDO versus glycerol conversion and (**b**) 1,2-PDO yield versus glycerol conversion.

inexpensive, and the activity of $CoCu/TiO_2$ can be further improved by fine-tuning the Co-to-Cu-to-TiO_2 ratio and optimizing the product formation using design of experiments.

Conclusion

The $15Co0.5Cu/TiO_2$ catalyst was highly active for the hydrogenolysis of glycerol to 1,2-PDO and has potential for industrial use. The maximum 1,2-PDO yield was achieved at 69.5% with 95.2% glycerol conversion and 73.0% 1,2-PDO selectivity under the maximized conditions of a catalyst-to-glycerol ratio of 0.028 and a reaction temperature of 250 °C at 4 MPa H_2 for 4 h. The addition of Cu to Co/TiO_2 caused a synergistic catalytic effect between the Co and Cu, providing much higher activity for 1,2-PDO formation than from the monometallic catalysts. The NH_3-TPD and H_2-TPR analyses suggested that an increase in the number of acid sites (especially weak acid sites) and the presence of multiple Co sites, respectively, can favor the hydrogenolysis of glycerol to 1,2-PDO. In the study on the effects of operating conditions, increasing the reaction temperature, initial pressure, and reaction time increased the glycerol conversion but decreased the selectivity to 1,2-PDO due to the degradation of formed 1,2-PDO to lower alcohols (1-propanol and 2-propanol).

Received: 20 September 2021; Accepted: 15 November 2021
Published online: 29 November 2021

References

1. Wang, Y., Zhou, J. & Guo, X. Catalytic hydrogenolysis of glycerol to propanediols: a review. *RSC Adv.* **5**, 74611–74628 (2015).

2. Anitha, M., Kamarudin, S. K. & Kofli, N. T. The potential of glycerol as a value-added commodity. *Chem. Eng. J.* **295**, 119–130 (2016).
3. Neves, T. M. *et al.* Glycerol dehydration over micro- and mesoporous ZSM-5 synthesized from a one-step method. *Microporous Mesoporous Mater.* **275**, 244–252 (2019).
4. Polychronopoulou, K. *et al.* Ce–Sm–xCu cost-efficient catalysts for H_2 production through the glycerol steam reforming reaction. *Sustain. Energ. Fuels* **3**, 673–691 (2019).
5. Zhao, Z. *et al.* Volcano-shape glycerol oxidation activity of palladium-decorated gold nanoparticles. *Chem. Sci.* **5**, 3715–3728 (2014).
6. Mitta, H., Seelam, P. K., Ojala, S., Keiski, R. L. & Balla, P. Tuning Y-zeolite based catalyst with copper for enhanced activity and selectivity in vapor phase hydrogenolysis of glycerol to 1,2-propanediol. *Appl. Catal. A: Gen.* **550**, 308–319 (2018).
7. Feng, Y. S. *et al.* Selective hydrogenolysis of glycerol to 1,2-propanediol catalyzed by supported bimetallic PdCu-KF/γ-Al_2O_3. *Chem. Eng. J.* **281**, 96–101 (2015).
8. Li, X., Xiang, M. & Wu, D. Hydrogenolysis of glycerol over bimetallic Cu Ni catalysts supported on hierarchically porous SAPO-11 zeolite. *Catal. Commun.* **119**, 170–175 (2019).
9. Lee, M., Hwang, Y. K., Chang, J. S., Chae, H. J. & Hwang, D. W. Vapor-phase hydrogenolysis of glycerol to 1,2-propanediol using a chromium-free Ni-Cu-SiO_2 nanocomposite catalyst. *Catal. Commun.* **84**, 5–10 (2016).
10. Cai, F., Jin, F., Hao, J. & Xiao, G. Selective hydrogenolysis of glycerol to 1,2-propanediol on Nb-modified Pd–Zr–Al catalysts. *Catal. Commun.* **131**, (2019).
11. Kant, A. *et al.* Hydrogenolysis of glycerol over Ni, Cu, Zn, and Zr supported on H-beta. *Chem. Eng. J.* **317**, 1–8 (2017).
12. Filonenko, G. A., van Putten, R., Hensen, E. J. M. & Pidko, E. A. Catalytic (de)hydrogenation promoted by non-precious metals–Co, Fe and Mn: recent advances in an emerging field. *Chem. Soc. Rev.* **47**, 1459–1483 (2018).
13. Guo, X. *et al.* Co/MgO catalysts for hydrogenolysis of glycerol to 1,2-propanediol. *Appl. Catal. A Gen.* **371**, 108–113 (2009).
14. Rekha, V., Sumana, C., Douglas, S. P. & Lingaiah, N. Understanding the role of Co in Co–ZnO mixed oxide catalysts for the selective hydrogenolysis of glycerol. *Appl. Catal. A Gen.* **491**, 155–162 (2015).
15. Feng, J. *et al.* Hydrogenolysis of glycerol to glycols over ruthenium catalysts: Effect of support and catalyst reduction temperature. *Catal. Commun.* **9**, 1458–1464 (2008).
16. Salazar, J. B. *et al.* Selective production of 1,2-propanediol by hydrogenolysis of glycerol over bimetallic Ru–Cu nanoparticles supported on TiO_2. *Appl. Catal. A Gen.* **482**, 137–144 (2014).
17. Regue, M. *et al.* Mo-doped TiO_2 photoanodes using $[Ti_4Mo_2O_8(OEt)_{10}]_2$ bimetallic oxo cages as a single source precursor. *Sustain. Energ. Fuels* **2**, 2674–2686 (2018).
18. Huang, Z. *et al.* Hydrogenation of γ-butyrolactone to 1,4-butanediol over CuCo/TiO_2 bimetallic catalysts. *ACS Catal.* **7**, 8429–8440 (2017).
19. Lee, J. C., Gopalan, A. I., Saianand, G., Lee, K. P. & Kim, W. J. Manganese and graphene included titanium dioxide composite nanowires: Fabrication, characterization and enhanced photocatalytic activities. *Nanomaterials* **10**, 456 (2020).
20. Li, S. *et al.* Effect of Cu substitution on promoted benzene oxidation over porous CuCo-based catalysts derived from layered double hydroxide with resistance of water vapor. *Appl. Catal. B Environ.* **166**, 260–269 (2015).
21. Raju, N. *et al.* Studies on continuous selective hydrogenolysis of glycerol over supported Cu–Co bimetallic catalysts. *New J. Chem.* **44**, 3122–3128 (2020).
22. Thongboon, S., Rittiron, P., Kiatsaengthong, D., Chukeaw, T. & Seubsai, A. Propylene epoxidation to propylene oxide over RuO_2, CuO, TeO_2, and TiO_2 supported on modified mesoporous silicas. *J. Nanosci. Nanotechnol.* **20**, 3466–3477 (2020).
23. Buttersack, C. Modeling of type IV and V sigmoidal adsorption isotherms. *Phys. Chem. Chem. Phys.* **21**, 5614–5626 (2019).
24. Gu, S. *et al.* Effects of metal or metal oxide additives on oxidative coupling of methane using Na_2WO_4/SiO_2 catalysts: Reducibility of metal additives to manipulate the catalytic activity. *Appl. Catal. A: Gen.* **562**, 114–119 (2018).
25. Guo, X., Li, Y., Song, W. & Shen, W. Glycerol hydrogenolysis over Co catalysts derived from a layered double hydroxide precursor. *Catal. Lett.* **141**, 1458–1463 (2011).
26. Wei, Y. *et al.* Synthesis of Cu–Co catalysts for methanol decomposition to hydrogen production via deposition–precipitation with urea method. *Catal. Lett.* **149**, 2671–2682 (2019).
27. Abbas, M., Chen, Z., Zhang, J. & Chen, J. Highly dispersed, ultra-small and noble metal-free Cu nanodots supported on porous SiO_2 and their excellent catalytic hydrogenation of dimethyl oxalate to methyl glycolate. *New J. Chem.* **42**, 10290–10299 (2018).
28. Sun, K. *et al.* Synergetic catalysis of bimetallic copper-cobalt nanosheets for direct synthesis of ethanol and higher alcohols from syngas. *Catal. Sci. Technol.* **8**, 3936–3947 (2018).
29. Wu, G., Guan, N. & Li, L. Low temperature CO oxidation on Cu–Cu_2O/TiO_2 catalyst prepared by photodeposition. *Catal. Sci. Technol.* **1**, 601–608 (2011).
30. Li, Z. *et al.* High-performance CoCu catalyst encapsulated in KIT-6 for higher alcohol synthesis from syngas. *ACS Sustain. Chem. Eng.* **8**, 200–209 (2019).
31. Liang, J. *et al.* Improved conversion of stearic acid to diesel-like hydrocarbons by carbon nanotubes-supported CuCo catalysts. *Fuel Process. Technol.* **188**, 153–163 (2019).
32. Sepúlveda, C. *et al.* The promoter effect of Co on the catalytic activity of the Cu oxide active phase supported on Al_2O_3 in the hydrogenolysis of glycerol. *New J. Chem.* **43**, 15636–15645 (2019).
33. Pudi, S. M., Biswas, P. & Kumar, S. Selective hydrogenolysis of glycerol to 1,2-propanediol over highly active copper–magnesia catalysts: Reaction parameter, catalyst stability and mechanism study. *J. Chem. Technol.* **91**, 2063–2075 (2016).
34. Amada, Y. *et al.* Reaction mechanism of the glycerol hydrogenolysis to 1,3-propanediol over Ir–ReO_x/SiO_2 catalyst. *Appl. Catal. B: Environ.* **105**, 117–127 (2011).
35. Zhou, J., Guo, L., Guo, X., Mao, J. & Zhang, S. Selective hydrogenolysis of glycerol to propanediols on supported Cu-containing bimetallic catalysts. *Green Chem.* **12**, 1835–1843 (2010).
36. Pandhare, N. N., Pudi, S. M., Biswas, P. & Sinha, S. Vapor phase hydrogenolysis of glycerol to 1,2-propanediol over γ-Al_2O_3 supported copper or nickel monometallic and copper–nickel bimetallic catalysts. *J. Taiwan Inst. Chem. Eng.* **61**, 90–96 (2016).
37. Mondal, S., Janardhan, R., Meena, M. L. & Biswas, P. Highly active Cu-Zn-Mg-Al-O catalyst derived from layered double hydroxides (LDHs) precursor for selective hydrogenolysis of glycerol to 1,2-propanediol. *J. Environ. Chem. Eng.* **5**, 5695–5706 (2017).
38. Li, K. T., Wang, C. H. & Wang, H. C. Hydrogenolysis of glycerol to 1,2-propanediol on copper core-porous silica shell-nanoparticles. *J. Taiwan Inst. Chem. Eng.* **52**, 79–84 (2015).

Acknowledgements

This research work was funded by: the Faculty of Engineering at Kasetsart University, Bangkok, Thailand; the Kasetsart University Research and Development Institute (KURDI); the Center of Excellence on Petrochemical and Materials Technology, Thailand; and the National Nanotechnology Center (NANOTEC), NSTDA, Ministry of Science and Technology, Thailand, through its Research Network program NANOTEC (RNN).

Author contributions

W.M., S.C., and P.S. conducted the experiments and prepared the manuscript. T.W., M.C., K.F., and H.S. consulted the results, provided resources, and proofed the manuscript. A.S. supervised all the work and prepared the manuscript text. All authors reviewed the manuscript.

Funding

Faculty of Engineering at Kasetsart University, National Nanotechnology Center, Center of Excellence on Petrochemical and Materials Technology, Kasetsart University Research and Development Institute.

Competing interests

The authors declare no competing interests.

Additional information

Supplementary Information The online version contains supplementary material available at https://doi.org/10.1038/s41598-021-02416-7.

Correspondence and requests for materials should be addressed to A.S.

Reprints and permissions information is available at www.nature.com/reprints.

Publisher's note Springer Nature remains neutral with regard to jurisdictional claims in published maps and institutional affiliations.